Mechanism for bipolar switching in a Pt/TiO_2/Pt resistive switching cell

Doo Seok Jeong,* Herbert Schroeder, and Rainer Waser
Research Center Jülich, Institute of Solid State Research and JARA-Fundamentals of Future Information Technology, Jülich D-52425, Germany

(Received 15 January 2009; revised manuscript received 11 March 2009; published 18 May 2009)

We suggest a possible mechanism for bipolar switching in a Pt/TiO_2/Pt resistive switching cell in terms of electrochemical reactions involving oxygen ions/vacancies. The electrochemical reactions are considered to take place at an interface between Pt and TiO_2 solid electrolyte, and they modulate the Schottky barrier height at the interface. Calculation results using this proposed mechanism can explain a bipolar switching behavior and semiquantitatively describe experimental data.

DOI: 10.1103/PhysRevB.79.195317 PACS number(s): 73.40.Rw, 77.55.+f, 77.84.Dy, 73.25.+i

I. INTRODUCTION

Recently, bipolar switching in oxide materials such as TiO_2 (Refs. 1–3), and $SrTiO_3$ (Refs. 4 and 5) has been vigorously investigated for application to resistive random access memory (RRAM) devices. The possible application of the oxide materials has attracted interest in an increased database as well as a mechanism for the bipolar switching. For TiO_2, experiments reveal several evidence about possible mechanisms of electroforming and bipolar switching, but there has been no theoretical description about them. Because of the dependence of bipolar switching on the polarity of electroforming voltage,[6] it is usually assumed that bipolar switching involves the migration of charged particles, most probably ions. Furthermore, the evolution of gas bubbles at the anode of a Pt/TiO_2/Pt switching cell was observed during electroforming, possibly indicating the electrochemical formation of oxygen gas. Therefore, bipolar switching in TiO_2 has been categorized as anion (or anion vacancy)-migration-induced switching.[7] In spite of this categorization, the role of oxygen ions/vacancies in bipolar switching mechanism needs more elaboration.

TiO_2 is regarded as solid electrolyte[8] so that defective TiO_{2-x} is believed to show a higher ionic contribution to the electrical current compared to stoichiometric TiO_2. It has been reported that oxygen vacancies in TiO_2 give rise to delocalized conduction electrons rather than localized in-gap states[9,10] so that all the oxygen vacancies in TiO_{2-x} are ionized and can serve as mobile space charges. Due to their low diffusivity or mobility, a quasistatic approximation cannot be applied to the calculation of oxygen-vacancy distribution so that one should evaluate the distribution in a time domain. The applied voltage is an important factor leading to the redistribution of oxygen vacancies, and thus the distribution needs to be determined in a time domain at various voltages. According to the Poisson equation, the time-dependent redistribution of oxygen vacancies under a certain voltage leads to a change in the voltage distribution in TiO_{2-x}, implying a change in the profile of the conduction and valence bands. And the change might vary electron-transport behavior in turn, giving rise to a change in the resistance with respect to time. It is therefore necessary for the understanding of the time-dependent bipolar switching behavior to look into the time-dependent distribution of oxygen vacancies and electrons.

When the interface between metal and electrolyte is dealt with, the Helmholtz layer should be taken into account. The Helmholtz layer is formed due to the separation of two oppositely charged layers, one is on the metal side and the other on the electrolyte side at the interface.[11] Considering high electron density in the metal, electric field screening length is estimated to be very short. Furthermore, the size of an electron is very small compared with ions so that a charged layer on the metal side must be placed only at the interface without remarkable electric field penetration into the metal. However, the ions taking part in electric field screening in the electrolyte have a finite size, and thus the distance between the charged layer on the metal side and the center of the ions is at least the radius of the ions. The plane passing through the centers of the ions nearest to the interface is termed the Helmholtz plane and the layer between the interface and the Helmholtz plane is termed the Helmholtz layer.

In fact, in metal/electrolyte junction not only the Helmholtz layer but also the Gouy-Chapman (diffuse) layer is in charge of electric field screening on the electrolyte side.[11] The Gouy-Chapman layer is composed of the ions screening the electric field penetrating into the electrolyte. It is formed behind the Helmholtz layer. However, it is not necessarily formed in solid electrolyte because of the low diffusivity of ions in solid electrolyte.

In this paper, we suggest a mechanism for bipolar switching in Pt/TiO_2/Pt in terms of the modulation of the Schottky barrier height (SBH) at one interface due to the voltage- and time-dependent variation in space charges composed of oxygen vacancies and electrons close to the interface. As a matter of fact, a change in the SBH of metal-oxide junction due to oxygen vacancies has been demonstrated using first-principles calculations.[12] Electrochemical reactions involving oxygen vacancies at a Pt/TiO_{2-x} interface are defined by taking into account the Helmholtz layer at the interface. Due to a large voltage drop in the Helmholtz layer and under the assumption that the Helmholtz layer is thin enough to be transparent for electrons, we can describe the modulation of the SBH in terms of the variation in the internal electric field in the Helmholtz layer. Electrons injected from the cathode see a reduced SBH which is the energy difference between the work function of the cathode and the conduction-band minimum of TiO_{2-x} at the Helmholtz layer/TiO_{2-x} interface.

The time-dependent distribution of oxygen vacancies can be obtained by solving the drift-diffusion equation and Fick's

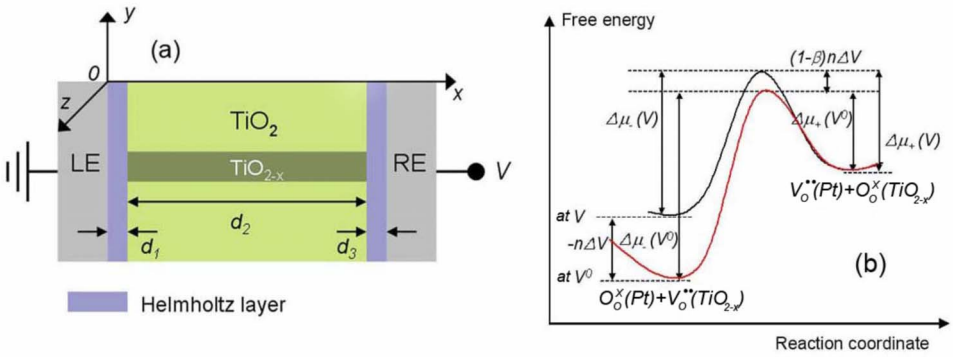

FIG. 1. (Color online) (a) Configuration of a TiO_2 switching cell. (b) Free-energy diagram of Eq. (1a) with respect to a reaction coordinate. The lower and upper lines denote diagrams at applied voltages of V^0 (reference voltage) and V $(=V^0+\Delta V)$, respectively. $\Delta\mu_-$ and $\Delta\mu_+$ are energy barrier heights for the forward and the reverse reactions, respectively. β means the asymmetry factor.

second law using proper boundary conditions. For simplicity, the entire calculation in this paper is performed on a simplified one-dimensional $Pt/TiO_{2-x}/Pt$ junction without taking into account a real three-dimensional configuration of a TiO_{2-x} phase in TiO_2. The $Pt/TiO_{2-x}/Pt$ system is assumed to be isolated from the ambient atmosphere so that no exchange of oxygen is considered. This deviation from the reality might hinder accounting for many experimental observations such as long data retention, endurance, switching speed. Nevertheless, the mechanism suggested in this paper is very meaningful as a prototype of an anion-reaction-induced bipolar switching mechanism. The calculation is performed using a finite difference method.

II. MODELING OF BIPOLAR SWITCHING BEHAVIOR

A. Electrochemical reaction through the Helmholtz layer

The Helmholtz layer is supposed to be formed at a Pt/TiO_{2-x} interface due to the separation of two oppositely charged layers, one is on the Pt side and the other is on the TiO_{2-x} side. Electroforming has been found to lead to the incorporation of oxygen into the Pt electrode,[6] most probably at grain boundaries in Pt by chemisorption or physisorption. It can be speculated that oxygen atoms in Pt can take part in the voltage-controlled electrochemical reaction of the formation and annihilation of oxygen vacancies at a Pt/TiO_{2-x} interface. In this study, the oxygen ions are assumed to have a charge of −2 in Pt. Since now we describe all the electrochemical reactions using the Kröger-Vink notation representing relative charges. With the Kröger-Vink notation, an oxygen-vacancy annihilation reaction on the TiO_{2-x} side of the interface is given by

$$O_O^{\times}(\mathrm{Pt}) + V_O^{\bullet\bullet}(TiO_{2-x}) \rightarrow V_O^{\bullet\bullet}(\mathrm{Pt}) + O_O^{\times}(TiO_{2-x}), \quad (1a)$$

where Pt and TiO_{2-x} in the parentheses indicate where the given relative charges are present. The reverse of Eq. (1a) indicates an oxygen-vacancy formation reaction on the TiO_{2-x} side. Concerning the formation free energy of Eq. (1a), the reaction can be divided into three reactions.

$$O_O^{\times}(\mathrm{Pt}) \rightarrow V_O^{\bullet\bullet}(\mathrm{Pt}) + 2e^-(\mathrm{Pt}) + 1/2O_{2(g)}, \quad (1b)$$

$$1/2O_{2(g)} + V_O^{\bullet\bullet}(TiO_{2-x}) + 2e^-(TiO_{2-x}) \rightarrow O_O^{\times}(TiO_{2-x}), \quad (1c)$$

and

$$e^-(\mathrm{Pt}) \rightarrow e^-(TiO_{2-x}). \quad (1d)$$

Free electrons in Pt should be distinguished from those in TiO_{2-x} because of the difference of the work functions of Pt and TiO_{2-x}. A first-principles study on oxygen chemisorption at a Pt surface has shown that the formation energy of oxygen chemisorption per oxygen atom is −1.57 eV.[13] Therefore, a change in the energy of Eq. (1b) is considered to be 1.57 eV. A free-energy change of Eq. (1c) in TiO_2 has been frequently evaluated by measuring a conductivity change with respect to temperature. Balachandra *et al.*[14] have evaluated a energy change in Eq. (1c) in nonstoichiometric TiO_{2-x}, which is approximately −2.1 eV. A change in energy of Eq. (1d) can be determined from the work-function difference between Pt and TiO_{2-x}. Due to electroforming-induced heavy self-doping with oxygen vacancies, the Fermi energy of TiO_{2-x} is believed to be very close to the conduction-band minimum, thus the work-function difference between Pt and TiO_{2-x} is approximately $\phi_m - \chi_{TiO_{2-x}}$, where ϕ_m and $\chi_{TiO_{2-x}}$ are the work function of Pt and the electron affinity of TiO_{2-x}, respectively. Therefore, the energy for Eq. (1d) is equal to $\phi_m - \chi_{TiO_{2-x}}$.

Figure 1(a) depicts the configuration of a $Pt/TiO_2/Pt$ switching cell including a conduction path composed of a TiO_{2-x} phase in insulating matrix, TiO_2. As will be discussed in Sec. II D, the cross section of the conduction path shown in Fig. 1(a) is estimated to be approximately a few tens μm^2. The interface reaction [Eq. (1a)] at one of the two interface of the $Pt/TiO_2/Pt$ cell will be dominant, which then is termed the *active* interface determined by the polarity of electroforming voltage.[6] A free-energy diagram of the assumed reaction is depicted in Fig. 1(b). As shown, the energies of oxygen ions and vacancies at a Pt/TiO_{2-x} interface rely on the applied voltage so that the applied voltage varies the activation energies for the oxygen-vacancy formation and annihilation reactions. Consequently, the reaction-rate constant of the forward and reverse reactions is given by a func-

tion of the applied voltage. The formation free energy of Eq. (1a) is expressed as

$$\Delta\mu = \Delta\mu^0 + k_B T \ln \frac{\bar{c}_{O(TiO_{2-x})}\bar{c}_{V(Pt)}}{\bar{c}_{V(TiO_{2-x})}\bar{c}_{O(Pt)}}, \tag{2}$$

where

$$\Delta\mu^0 = \mu^0_{O(TiO_{2-x})} + \mu^0_{V(Pt)} - \mu^0_{V(TiO_{2-x})} - \mu^0_{O(Pt)} = \Delta h - T\Delta s. \tag{3}$$

k_B and T are the Boltzmann constant and temperature, respectively. μ_i^0, where $i \in \{O(TiO_{2-x}), O(Pt), V(TiO_{2-x}), V(Pt)\}$, denotes the standard chemical potential of $O_O^\times$ and $V_O^{\bullet\bullet}$ placed in TiO_{2-x} and Pt. Δh and Δs denote changes in the enthalpy and entropy, respectively, for the reaction in Eq. (1a). $\bar{c}_i$, where $i \in \{O(TiO_{2-x}), O(Pt), V(TiO_{2-x}), V(Pt)\}$, is a ratio of concentration c_i to c_i^0 in the standard state, c_i/c_i^0. The standard state means a pure state so that c_O^0 is equal to c_V^0. Therefore, the ratio $\bar{c}_{O(TiO_{2-x})}\bar{c}_{V(Pt)}/\bar{c}_{V(TiO_{2-x})}\bar{c}_{O(Pt)}$ can be rewritten by

$$\frac{\bar{c}_{O(TiO_{2-x})}\bar{c}_{V(Pt)}}{\bar{c}_{V(TiO_{2-x})}\bar{c}_{O(Pt)}} = \frac{[c^0_{O(Pt)} - c_{O(Pt)}][c^0_{O(TiO_{2-x})} - c_{V(TiO_{2-x})}]}{c_{V(TiO_{2-x})}c_{O(Pt)}}. \tag{4}$$

Consequently, the Nernst potential V_n of Eq. (1a) is given by

$$V_n = \frac{1}{n}(\Delta h - T\Delta s) + \frac{k_B T}{n}\ln\frac{[c^0_{O(Pt)} - c_{O(Pt)}][c^0_{O(TiO_{2-x})} - c_{V(TiO_{2-x})}]}{c_{V(TiO_{2-x})}c_{O(Pt)}}, \tag{5}$$

where n means the ionization number of O.

Concerning the kinetics of Eq. (1a), the variation in the activation energies depicted in Fig. 1(b) with respect to the applied voltage can be explained as follows: the energy barrier per oxygen, O, for the reverse reaction of Eq. (1a) with a voltage at d_1 $[V(d_1)]$ is written by $\mu_+[V(d_1)]$. The difference in energy barrier height for the reverse reaction at two different voltages at d_1, $V(d_1)$, and $V^0(d_1)$, is expressed as

$$\Delta\mu_+[V(d_1)] - \Delta\mu_+[V^0(d_1)] = -(1-\beta)n\Delta V, \tag{6}$$

where ΔV is equal to $V(d_1) - V^0(d_1)$. Similarly, the difference in energy barrier heights for the forward reaction at $V(d_1)$ and $V^0(d_1)$ is expressed as

$$\Delta\mu_-[V(d_1)] - \Delta\mu_-[V^0(d_1)] = \beta n\Delta V. \tag{7}$$

Therefore, the flux equation of O undergoing the forward and the reverse reactions at the left electrode (LE)/TiO_{2-x} interface, i.e., J^0_{-L} and J^0_{+L}, are described by

$$J^O_{-L} = k_- c_{O(Pt)}c_{V(TiO_{2-x})}\exp\left(\frac{-\beta n\Delta V}{k_B T}\right), \tag{8}$$

and

$$J^O_{+L} = k_+ c_{O(TiO_{2-x})}c_{V(Pt)}\exp\left[\frac{(1-\beta)n\Delta V}{k_B T}\right], \tag{9}$$

respectively. k_- and k_+ are the rates of the forward and the reverse reactions, respectively. The overall flux equation of oxygen, J^O_L, is the summation of Eqs. (8) and (9).

$$J^O_L = k_- c_{O(Pt)}c_{V(TiO_{2-x})}\exp\left(\frac{-\beta n\Delta V}{k_B T}\right) - k_+ c_{O(TiO_{2-x})}c_{V(Pt)}\exp\left[\frac{(1-\beta)n\Delta V}{k_B T}\right]. \tag{10}$$

By taking $V^0(d_1)=0$ as a reference voltage and using k_-^0 and k_+^0, the forward and the reverse reaction-rate constants at the reference voltage, Eq. (10) can be rewritten by

$$J^O_L = k^0_- c_{O(Pt)}c_{V(TiO_{2-x})}\exp\left[\frac{-\beta nV(d_1)}{k_B T}\right] - k^0_+ c_{O(TiO_{2-x})}c_{V(Pt)}\exp\left[\frac{(1-\beta)nV(d_1)}{k_B T}\right]. \tag{11}$$

In equilibrium, J^0_{-L} is equal to J^0_{+L}, so that the net flux is zero. The voltage at d_1 in equilibrium is defined as the Nernst potential V_n. V_n can therefore be given by

$$V_n = \frac{k_B T}{n}\ln\frac{k^0_+}{k^0_-} + \frac{k_B T}{n}\ln\frac{c_{O(TiO_{2-x})}c_{V(Pt)}}{c_{O(Pt)}c_{V(TiO_{2-x})}}. \tag{12}$$

Comparing Eq. (12) with Eq. (5) gives the ratio k_+^0/k_-^0 as

$$\frac{k^0_+}{k^0_-} = \exp\left(\frac{-\Delta s}{k_B}\right)\exp\left(\frac{\Delta h}{k_B T}\right). \tag{13}$$

The flux equation of the forward/reverse reaction at V_n (J^0) can be obtained by entering Eq. (13) into Eq. (11), giving the following equation:

$$J^0 = k^0_-\left(\frac{k^0_+}{k^0_-}\right)^\beta \frac{[c_{O(TiO_{2-x})}c_{V(Pt)}]^\beta}{[c_{O(Pt)}c_{V(TiO_{2-x})}]^{\beta-1}}. \tag{14}$$

Therefore, the net flux equation for oxygen, O, can be written by a form of the Butler-Volmer equation,[9]

$$J^O_L = J^0\left[1 - \exp\left\{\frac{n[V(d_1) + V_n]}{k_B T}\right\}\right]\exp\left\{\frac{-\beta n[V(d_1) - V_n]}{k_B T}\right\}. \tag{15}$$

For the Helmholtz layer at the TiO_{2-x}/right electrode (RE) interface an oxygen ion flux equation J^O_R can be derived using the same procedure as used for the J^O_L, and is given by

$$J^O_R = J^0\left[1 - \exp\left\{-\frac{n[V_{ap} - V(d_1+d_2) - V_n]}{k_B T}\right\}\right] \times \exp\left\{\frac{\beta n[V_{ap} - V(d_1+d_2) - V_n]}{k_B T}\right\}. \tag{16}$$

Equations (15) and (16) will serve as boundary conditions for the calculation of the time-dependent distribution of oxygen vacancies.

B. Drift diffusion of oxygen vacancies and electrons in TiO_{2-x}

TiO_{2-x} is estimated to be n-type semiconductor as electroforming is expected to introduce a large amount of oxygen vacancies in TiO_{2-x}. Electrons and oxygen vacancies are regarded as majority charged particles in TiO_{2-x}. The one-dimensional time-dependent distribution of oxygen vacancies and electrons can be determined by solving the one-dimensional drift diffusion equation, given by

$$J_{DD}^{i} = z_i c_i \mu_i E - D_i \frac{\partial c_i}{\partial x}, \quad i \in \{e, V_O\}, \tag{17}$$

where z_i, μ_i, and D_i mean the charge number, the mobility, and the diffusivity of particle i, respectively. Equation (17) describes the flux of charged particle i due to drift and diffusion, whose driving forces are the electric field E and the concentration gradient of particle i, respectively. The electric field is attributed to the applied voltage and the internal electric field. By introducing the Fermi energy ε_F (electrochemical potential) into Eq. (17), the equation for electrons is rewritten by

$$J_{DD}^{e} = -c_e \mu_e \frac{d\varepsilon_F}{dx}. \tag{18}$$

Fick's second law is expressed as

$$\frac{\partial c_i}{\partial t} = -\frac{\partial J_{DD}^{i}}{\partial x}. \tag{19}$$

Entering Eq. (17) into Eq. (19) results in

$$\frac{\partial c_i}{\partial t} = -z_i c_i \mu_i \frac{\partial E}{\partial x} - z_i \mu_i E \frac{\partial c_i}{\partial x} + D_i \frac{\partial^2 c_i}{\partial x^2}. \tag{20}$$

In order to solve Eq. (20), one should evaluate E as a function of x. E is obtained by solving the Poisson equation with proper boundary conditions, which is given by $dE/dx = q\rho/\varepsilon_r\varepsilon_0$, where q, ε_r, and ε_0 are the elementary charge, the dielectric constant of TiO_{2-x}, and the permittivity of vacuum, respectively. ρ is equal to $\Sigma_i z_i c_i$, where $i \in \{e, V_O\}$. By integrating the Poisson equation over the range $d_1 \le x \le d_1 + d_2$, E and V at $x = d_1 + d_2$ can be calculated as the following equations:

$$E(d_1 + d_2) = E(d_1) + \frac{q}{\varepsilon_r \varepsilon_0} \int_{d_1}^{d_1+d_2} \rho(x) dx, \tag{21}$$

and

$$V(d_1 + d_2) = V(d_1) - E(d_1) d_2 - \frac{q}{\varepsilon_r \varepsilon_0} \int_{d_1}^{d_1+d_2} \int_{d_1}^{x} \rho(x') dx' dx. \tag{22}$$

On the assumption that electric field penetration depth (screening length) in Pt is very small so that a voltage drop in Pt is negligible, the applied voltage V_{ap} is equal to the summation of voltage drops in the left Helmholtz layer, TiO_{2-x}, and the right Helmholtz layer (V_1, V_2, V_3). Using the continuity equation, V_1 and V_3 can be expressed as $-d_1\varepsilon_r E(d_1)/\varepsilon_{rH}$ and $-d_3\varepsilon_r E(d_1+d_2)/\varepsilon_{rH}$, respectively. ε_{rH} means the dielectric constant of the Helmholtz layer. V_{ap} is therefore written by

$$V_{ap} = -\frac{d_1\varepsilon_r}{\varepsilon_{rH}} E(d_1) - \frac{d_3\varepsilon_r}{\varepsilon_{rH}} E(d_1 + d_2) + V(d_1 + d_2) - V(d_1). \tag{23}$$

Arranging Eq. (23) after entering Eqs. (21) and (22) into Eq. (23) gives $E(d_1)$ as expressed as

$$E(d_1) = -\frac{1}{d_1\varepsilon_r/\varepsilon_{rH} + d_2 + d_3\varepsilon_r/\varepsilon_{rH}} \times \left[V_{ap} + \frac{q d_3}{\varepsilon_{rH}\varepsilon_0} \int_{d_1}^{d_1+d_2} \rho(x) dx + \frac{q}{\varepsilon_r \varepsilon_0} \int_{d_1}^{d_1+d_2} \int_{d_1}^{x} \rho(x') dx' dx \right]. \tag{24}$$

Since $V(x)$ for $d_1 \le x \le d_1 + d_2$ is given by

$$V(x) = V(d_1) - E(d_1) d_2 - \frac{q}{\varepsilon_r \varepsilon_0} \int_{d_1}^{x} \int_{d_1}^{x'} \rho(x'') dx'' dx', \tag{25}$$

$V(x)$ can be evaluated by entering Eq. (24) into Eq. (25).

The calculation of the quasistatic distribution of electrons at given distribution of oxygen vacancies in a time domain can be performed with the voltage distribution along the TiO_{2-x} conduction path, determined from Eq. (25). The quasistatic calculation of the electron distribution will be verified to be reasonable in Sec. II C. As shown in Eq. (25), V is given by a function of ρ. Considering the electron contribution to ρ, where electrons satisfy the Fermi-Dirac statistics, ρ is a function of V. That is, Eq. (25) is a self-consistent equation so that solving the equation gives both V and ρ.

However, ρ is given by a function of V as well as the Fermi energy ε_F, namely, there are two variables in Eq. (25). One more equation for V and ρ therefore needs to be solved to evaluate their distribution. Equation (18) with proper boundary conditions can be that equation. As mentioned earlier, the electron concentration c_e in Eq. (18) is a function based on the Fermi-Dirac statistics, in which V and ε_F are the only variables. In a quasistatic state, electronic current density J_{DD}^{e} is constant along the direction x through the conduction path. Therefore, if J_{DD}^{e} at $x = d_1$, serving as a boundary condition, is known, $c_e\mu_e d\varepsilon_F/dx$ along the direction x can be evaluated. Therefore, Eq. (18) serves as the other equation for V and ρ so that the distribution of V and ρ is evaluated by solving the two simultaneous equations, Eqs. (18) and (25). However, it turns out that solving Eqs. (18) and (25) is impossible using an analytical calculation. Therefore, the finite difference method will be used to calculate the time-dependent distribution of electrons and oxygen vacancies, which will be explained in Sec. II C.

Proper boundary conditions are necessary to solve Eq. (18). For the calculation of the oxygen-vacancy distribution, the flux of oxygen vacancies at the LE/TiO_{2-x} and the TiO_{2-x}/RE interfaces (J_L^V and J_R^V) serve as the boundary conditions. Since J_L^V is equal to $-J_L^O$, the negative of Eqs. (15)

and (16) can be taken as boundary conditions. For the calculation of electron distribution, electronic current densities at the LE/TiO_{2-x} and the TiO_{2-x}/RE interfaces (J_L^e and J_R^e) are used as the boundary conditions. To calculate J_L^e, the current densities due to electron transfers LE→TiO_{2-x} (J_{LT}^e) and TiO_{2-x}→LE (J_{TL}^e) should be evaluated. J_{LT}^e can be expressed in terms of the SBH at the LE/TiO_{2-x} interface (ϕ_b^L) by integrating the product of the density of electrons at a given energy in the LE and the corresponding velocity over the energy higher than ϕ_b^L. The density of electrons is expressed as the density of states of the LE multiplied by the Fermi-Dirac distribution function.[15]

$$J_{LT}^e = \frac{A^* T^2}{N_c} \int_{\varepsilon_c(d_1)}^{\infty} \frac{N_c' \sqrt{\varepsilon}}{1 + \exp\left(\frac{\varepsilon - \varepsilon_{Fm}}{k_B T}\right)} d\varepsilon; \quad N_c' = \frac{\sqrt{2} m_e^{3/2}}{\hbar^3 \pi^2}, \tag{26}$$

where N_c is the effective density of states for electrons, which is given by $2(2\pi m_e k_B T/h^2)^{3/2}$. A^*, $\varepsilon_c(d_1)$, $\varepsilon_c(d)$, and ε_{Fm} denote the effective Richardson constant, the conduction-band edge energies at d_1 and d, and the Fermi energy of the LE, respectively. In a similar way, J_{TL}^e is given by a function similar to Eq. (26).

$$J_{TL}^e = q v_{TL} \int_{\varepsilon_c(d_1)}^{\infty} \frac{N_c' \sqrt{\varepsilon - \varepsilon_c(d_1)}}{1 + \exp\left[\frac{\varepsilon - \varepsilon_F(d_1)}{k_B T}\right]} d\varepsilon, \tag{27}$$

where $\varepsilon_F(d_1)$ and v_{TL} are the Fermi energy at d_1 and velocity of the electron transfer TiO_{2-x}→LE, respectively. By putting together Eqs. (26) and (27) J_L^e can be written by

$$J_L^e = -\frac{A^* T^2 N_c'}{N_c} \int_{\varepsilon_c(d_1)}^{\infty} \frac{\sqrt{\varepsilon}}{1 + \exp\left(\frac{\varepsilon - \varepsilon_{Fm}}{k_B T}\right)} d\varepsilon + q v_{TL} N_c' \int_{\varepsilon_c(d_1)}^{\infty} \frac{\sqrt{\varepsilon - \varepsilon_c(d_1)}}{1 + \exp\left[\frac{\varepsilon - \varepsilon_F(d_1)}{k_B T}\right]} d\varepsilon. \tag{28}$$

Concerning J_R^e, the electron transfers, RE→TiO_{2-x} and TiO_{2-x}→RE, contribute to J_{RT}^e and J_{TR}^e, respectively. Using the same procedure as for the derivation of J_L^e, J_R^e can be obtained as

$$J_R^e = -q v_{TR} N_c' \int_{\varepsilon_c(d_1+d_2)}^{\infty} \frac{\sqrt{\varepsilon - \varepsilon_c(d_1+d_2)}}{1 + \exp\left[\frac{\varepsilon - \varepsilon_F(d_1+d_2)}{k_B T}\right]} d\varepsilon + \frac{A^* T^2 N_c'}{N_c} \int_{\varepsilon_c(d_1+d_2)}^{\infty} \frac{\sqrt{\varepsilon}}{1 + \exp\left(\frac{\varepsilon - \varepsilon_{Fm} - qV_{ap}}{k_B T}\right)} d\varepsilon, \tag{29}$$

where v_{TR} means velocity of the electron transfer TiO_{2-x}→RE. $\varepsilon_c(d_1+d_2)$ and $\varepsilon_F(d_1+d_2)$ denote conduction-band edge energies and the Fermi energy at d_1+d_2, respectively.

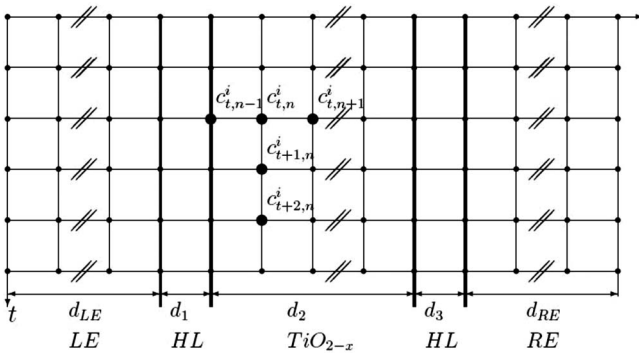

FIG. 2. Configuration of the nodes of Pt/TiO_{2-x}/Pt in two dimensions, time t and spatial coordinate x.

C. Finite difference method for the calculation

The explicit finite difference method (FDM) (Ref. 16) was chosen for the calculation of the drift-diffusion of oxygen vacancies and electrons in TiO_{2-x} and the formation and annihilation reactions of oxygen vacancies at the Helmholtz layer. Writing and compiling the code for this calculation were done using MATLAB™.

In the explicit FDM, Eq. (19) is given by the following equation:

$$\frac{c_{t,x}^i - c_{t-1,x}^i}{\Delta t} = \frac{1}{\Delta x}(j_{t-1,x-1/2}^i - j_{t-1,x+1/2}^i), \tag{30}$$

where $c_{t,x}^i$ denotes the concentration of particle i at time t and spatial point x and D_i its diffusivity. The configuration of the nodes in Pt/TiO_{2-x}/Pt is depicted in Fig. 2. Along the axis x, N_E, N_2, and N_E nodes are assigned to the LE, the TiO_{2-x} film, and the RE, respectively. d_E, d_1, d_2, and d_3 are the thicknesses of the LE (RE), the left Helmholtz layer, the TiO_{2-x} film, and the right Helmholtz layer, respectively. Therefore, the distance between neighboring nodes in the LE (RE) is $d_E/(N_E-1)$ and that in TiO_{2-x} is $d_2/(N_2-1)$. Along the axis t, N_t nodes are located with a distance between neighboring nodes of Δt. Let us start dealing with the drift diffusion of oxygen ions in the LE. Using the configuration of the nodes, Fick's second law of oxygen ions can be described as

$$\frac{c_{t+1,n}^{O(L)} - c_{t,n}^{O(L)}}{\Delta t} = \frac{N_E - 1}{d_E}(j_{t,n-1/2}^{O(L)} - j_{t,n+1/2}^{O(L)}), \tag{31}$$

where $c_{t,n}^{O(L)}$ is the concentration of oxygen ions at node (t,n) in the LE. Since an electric field is not present in metal, the drift of oxygen ions in the electrode can be ignored so that the oxygen ion flux equation due to only their diffusion at nodes $(t,n-1/2)$ and $(t,n+1/2)$ can be expressed as

$$J_{t,n-1/2}^{O(L)} = -\frac{D_O N_E}{d_E}(c_{t,n}^{O(L)} - c_{t,n-1}^{O(L)}), \tag{32}$$

and

$$J_{t,n+1/2}^{O(L)} = -\frac{D_O N_E}{d_E}(c_{t,n+1}^{O(L)} - c_{t,n}^{O(L)}), \tag{33}$$

respectively. Entering Eqs. (32) and (33) into Eq. (31) leads to the following equation:

$$c_{t+1,n}^{\mathrm{O}(L)} = c_{t,n}^{\mathrm{O}(L)} + \frac{D_{\mathrm{O}}(N_E-1)^2\Delta t}{d_E^2}(c_{t,n+1}^{\mathrm{O}(L)} - 2c_{t,n}^{\mathrm{O}(L)} + c_{t,n-1}^{\mathrm{O}(L)}). \tag{34}$$

Using Eq. (34), $c_{t+1,n}^{\mathrm{O}(L)}$ can be determined from $c_{t,n-1}^{\mathrm{O}(L)}$, $c_{t,n}^{\mathrm{O}(L)}$, and $c_{t,n+1}^{\mathrm{O}(L)}$. Net oxygen ion flux at the left end of the LE is assumed to be zero, implying oxygen ions coming into and out of the LE are in equilibrium. $J_{t,1/2}^{\mathrm{O}(L)}=0$ thus serves as a boundary condition. The other boundary condition at $N_E+1/2$ can be obtained from the net flux of the oxygen ions at the left Helmholtz layer given by Eq. (11). Therefore, $J_{t,N_E+1/2}^{\mathrm{O}(L)}$ is expressed as

$$J_{t,N_E+1/2}^{\mathrm{O}(L)} = k_-^0 c_{t,N_E}^{\mathrm{O}(L)} c_{t,1}^V \exp\left(-\frac{\beta n V_{t,1}}{k_B T}\right) - k_+^0 (c_{\mathrm{O}_\mathrm{O}^\times}^0 - c_{t,1}^V) \times (c_{\mathrm{O}(L)}^0 - c_{t,N_E}^{\mathrm{O}(L)}) \exp\left[\frac{(1-\beta) n V_{t,1}}{k_B T}\right]. \tag{35}$$

$c_{\mathrm{O}(L)}^0$ means the concentration of oxygen ions in the electrode in the standard state. A voltage at the node N_E of the LE is taken as a ground (zero). Considering the very short electric field screening length in metal, it is a reasonable assumption to ignore a voltage drop in the LE. Numbering the nodes in TiO_{2-x} is started from one at the left end of TiO_{2-x} without including the number of the nodes in the LE. $V_{t,1}$ denotes a voltage at $(t,1)$, which is at the interface between the left Helmholtz layer and TiO_{2-x}. $V_{t,1}$ will be determined using an iteration method for the calculation of electron concentration distribution in TiO_{2-x}. From the discrete diffusion equation and the boundary conditions oxygen distribution in the LE at each time node can be obtained with the proper initial distribution of oxygen.

Oxygen distribution in the RE and oxygen flux at the left and right ends are obtained using a similar derivation procedure that used for the calculation on the LE. However, boundary conditions at the left and right ends of the RE are the other way than those in the LE because the configuration of the RE is the mirror one of the LE. A boundary condition at the left end of the RE is given by

$$J_{t,1/2}^{\mathrm{O}(R)} = -k_-^0 c_{t,1}^{\mathrm{O}(R)} c_{t,N_2}^V \exp\left[-\frac{\beta n (V_{ap} - V_{t,N_2})}{k_B T}\right] + k_+^0 (c_{\mathrm{O}_\mathrm{O}^\times}^0 - c_{t,N_2}^V)(c_{\mathrm{O}(R)}^0 - c_{t,1}^{\mathrm{O}(R)}) \times \exp\left[\frac{(1-\beta) n (V_{ap} - V_{t,N_2})}{k_B T}\right] \tag{36}$$

Numbering the nodes in the RE is started from one at the interface between the right Helmholtz layer and the RE. Oxygen distribution in the RE can be obtained in the same manner as that in the LE.

The calculation of oxygen-vacancy and electron distribution in TiO_{2-x} is more complicated because both drift and diffusion of oxygen vacancies and electrons must be taken into account. The discrete drift-diffusion equation of particle i where $i \in \{e, V\}$ at nodes $(t,n+1/2)$ and $(t,n-1/2)$ can be expressed as

$$J_{t,n+1/2}^i = -\frac{1}{2d_2} z_i \mu_i (c_{t,n+1}^i + c_{t,n}^i)(N_2-1)(V_{t,n+1} - V_{t,n}) - \frac{N_2-1}{d_2} D_i (c_{t,n+1}^i - c_{t,n}^i) \tag{37}$$

and

$$J_{t,n-1/2}^i = -\frac{1}{2d_2} z_i \mu_i (c_{t,n}^i + c_{t,n-1}^i)(N_2-1)(V_{t,n} - V_{t,n-1}) - \frac{N_2-1}{d_2} D_i (c_{t,n}^i - c_{t,n-1}^i), \tag{38}$$

respectively. By entering Eqs. (37) and (38) into Fick's second law, $c_{t+1,n}^i$ can be expressed as a function of c^i and V at the nodes $(t,n-1)$, (t,n), and $(t,n+1)$. A voltage at each node can be evaluated by solving the Poisson equation, which needs space-charge density at every node. Therefore, $c_{t,n}^e$ and $c_{t,n}^V$ should be evaluated at all nodes n at time t.

Response of electrons to variations in the internal electric field is very fast compared to oxygen vacancies due to the higher mobility of the electrons. Therefore, very small time steps (~1 ps) must be used to evaluate time-dependent behavior of electrons. However, the drift diffusion of oxygen vacancies is very sluggish compared to electrons so that its time constant would be higher than a few hundreds μs relying on the low mobility of oxygen vacancies. Using then very small time steps (~1 ps) is not an efficient method because a huge amount of data points in the time domain are necessarily produced to calculate time-dependent drift diffusion of oxygen vacancies. Therefore, it is reasonable to use a more efficient quasistatic calculation for the evaluation of electron distribution and adequate larger time steps for the oxygen vacancies.

The calculated voltage distribution and electric field at the interface between the left Helmholtz layer and TiO_{2-x} in Eqs. (25) and (24), respectively, need to be written as proper forms in a discrete system. Space charge density ρ is defined as $\rho = 2c^V - c^e$. The integration $\int_{d_1}^{x} \rho(x)dx$ can be written using the trapezoidal rule[17] by

$$\int_{d_1}^{d_1+d_2(n-1)/N_2-1} \rho(x')dx' \approx \frac{d_2}{N_2-1}\left[\sum_{i=2}^{n-1} \rho(i) + \frac{1}{2}\rho(i=1) + \frac{1}{2}\rho(i=n)\right]. \tag{39}$$

By defining Eq. (39) as $f(i=n)$ the double integral on the right side of Eq. (25) can be replaced by

$$\int_{d_1}^{d_1+d_2(n-1)/N_2-1} f(x')dx' \approx \frac{d_2}{N_2-1}\left[\sum_{i=2}^{n-1} f(i) + \frac{1}{2}f(i=1) + \frac{1}{2}f(i=n)\right]. \tag{40}$$

The double integral in Eq. (24) is determined from Eq. (40) for $n=N_2$. Therefore, voltages at all nodes at time t at the

given distribution of space charges can be evaluated using the FDM.

The thickness of TiO_{2-x} (d_2) was set 50 nm. The total number of nodes in d_2 was 272. The variation in internal voltage and electron and oxygen-vacancy densities in the vicinity of the LE/TiO_{2-x} and TiO_{2-x}/RE interfaces is drastic compared with the bulk of the TiO_{2-x} film, thus 36 nodes were assigned to each near-interface region (within 2 nm distance from each interface) whereas 200 nodes the bulk of the film (46 nm). On the other hand, a homogeneous distribution of 199 nodes was given to each electrode because no internal electric field is expected in the LE and RE due to perfect electric field screening.

Since we deal with high electronic current density in the electroformed TiO_{2-x}, displacement current attributed to space-charge redistribution in TiO_{2-x} can be neglected. Therefore, drift-diffusion current in Eq. (17) for electrons is constant along the axis x at time t. In a discrete system Eq. (18) is expressed as $J_{DD}^{e}=-c_e^{t,i}\mu_e(E_F^{t,i+1}-E_F^{t,i})/\Delta x$, where the superscripts t and i denote time and location (ith node), respectively. Therefore, $E_F^{t,i+1}$ is determined from $E_F^{t,i}$ and $c_e^{t,i}$ because J_{DD}^{e} is constant at all the nodes, that is, $E_F^{t,i+1}$ is a dependent variable on $E_F^{t,i}$ and $c_e^{t,i}$. Using the Newton iteration[17] the voltage distribution in TiO_{2-x} as well as the Fermi energy distribution in the Pt/TiO_{2-x}/Pt configuration [shown in Fig. 1(a)] at given voltage and time could be calculated.

From the discussion up to now, the densities of oxygen vacancies and electrons could be defined at all locations (nodes n) at time t, thus time-dependent electronic and ionic current can be evaluated.

D. Calculation results

The symmetry of electroforming in TiO_2 is regarded to be determined by the polarity of the applied voltage for electroforming.[6] During electroforming the following reaction is expected to take place at the anode of Pt/TiO_2/Pt, $O_O^{\times}\rightarrow V_O^{\bullet\bullet}+2e^{-}+1/2O_2(g)$, with introducing a large amount of oxygen vacancies. In order to define an initial distribution of oxygen vacancies for the bipolar switching calculation, it was assumed that electroforming was performed by applying a negative voltage to the RE so that oxygen vacancies formed at the LE (anode)/TiO_{2-x} interface migrated to the RE and are accumulated. The accumulation of oxygen vacancies resulted in the growth of a conducting path composed of an oxygen-deficient phase, thus the oxygen-vacancy density profile after the electroforming process is qualitatively speculated to be like Fig. 3(a). The densities at d_1 and d_1+d_2 in the initial density profile are 10^{21} and 2.66×10^{21} cm^{-3}, respectively. The corresponding band diagram is shown in Fig. 3(b).

Assuming a prior electroforming process, the LE/TiO_{2-x} interface was assumed as the active interface (anode during the prior electroforming) for the electrochemical reaction shown in Eq. (1a), whereas the other interface was considered to be inactive with a low rate constant in Eq. (1a). This leads to a change in the oxygen-vacancy density at mainly the LE/TiO_{2-x} interface. The parameters used for the calculation of current density-voltage (J-V) curves are given in Table I. The Helmholtz layer is believed to be similar to an interfacial dipole layer in semiconductor physics.[18] ε_{rH} was assumed to be 7 as Black *et al.*[19] suggested in their paper. Regarding the thickness of the Helmholtz layer, it is ideally equal to the radius of the ions taking part in electric field screening. In this study, we regard oxygen vacancies to be in charge of the screening so that the radius of oxygen vacancies corresponds to the Helmholtz layer thickness. However, it is difficult to define the size of oxygen vacancies because they are effective ions rather than real ones. We thus assume the thickness of the Helmholtz layer to be 0.2 nm, approximately half the a-axis lattice constant of anatase TiO_2. As a matter of fact, the Helmholtz layer thickness plays a crucial role in the determination of the SBH. The SBH is determined from a voltage drop in the Helmholtz layer that is proportional to the Helmholtz layer thickness. The diffusivity of oxygen vacancies was set 10^{-18} cm^2 s^{-1}. As a matter of fact, the diffusivity at room temperature has been barely reported. The diffusivity used for this calculation was extrapolated from diffusivities measured at high temperatures

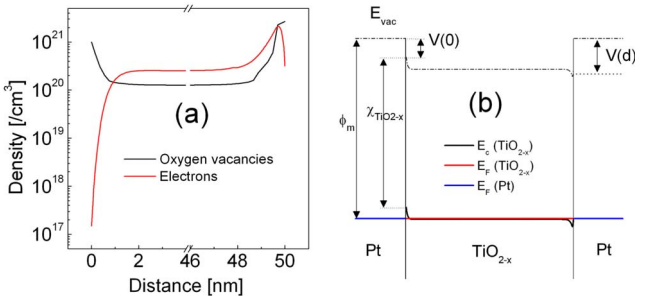

FIG. 3. (Color online) (a) Initial distribution of oxygen vacancies and free electrons in TiO_{2-x} between LE and RE. (b) Calculated band diagram of a Pt/TiO_{2-x}/Pt junction. $V(0)$ and $V(d)$ denote voltage drops in the left and the right Helmholtz layers, respectively.

TABLE I. Parameters for the bipolar switching simulation

Parameter	Value	Parameter	Value
D_V	10^{-18} cm^2 s^{-1} (Ref. 20)	β	0.45
D_O	10^{-15} cm^2 s^{-1} (Ref. 21)	n	−2
d_E	70 nm	Δh	0.75 eV
d_1	2 Å	s	1.2 meV/K
d_2	50 nm	$c_{O_O^{\times}}^{0}$	10^{23} cm^{-3}
d_3	2 Å	ε_r	20 (Ref. 22)
N_E	199	ε_{rH}	7 (Ref. 19)
N_2	272	ϕ_b	0.5 eV
N_t	5	m_e	13 m_0 (Ref. 23)
Δt	20 ms	A^*	1.2×10^6 A m^{-2} K^{-2} (Ref. 24)
k_-^0 at d_1	10^{-36} cm^4 s^{-1}	T	298 K
k_-^0 at d_1+d_2	10^{-62} cm^4 s^{-1}		

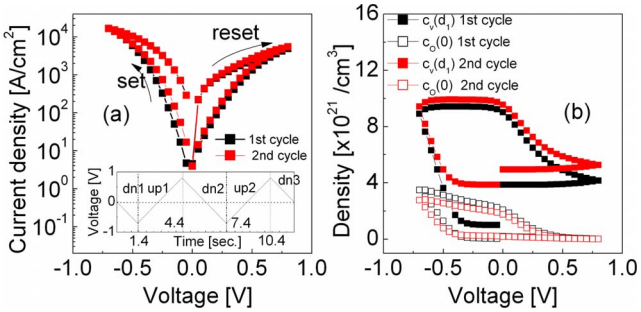

FIG. 4. (Color online) (a) Simulated J-V curves with the applied voltage cycles shown in the inset and a voltage delay time of 0.1 s. (b) Variation in oxygen-vacancy density on the TiO_{2-x} side and oxygen ion density on the LE side of the LE/TiO_{2-x} interface with respect to the applied voltage cycles. The mobility of oxygen vacancies was assumed to be 3.87×10^{-17} $cm^2/V\,s$ corresponding to a diffusivity of 10^{-18} cm^2/s (Ref. 20). A voltage sweep rate was 0.5 V/s.

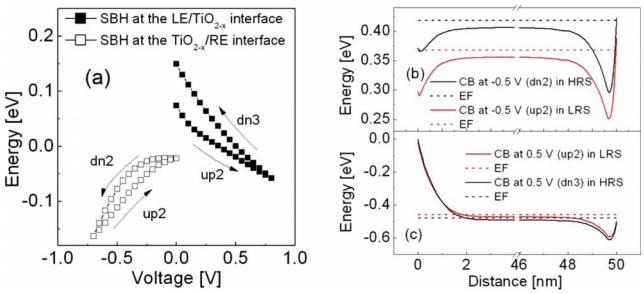

FIG. 5. (Color online) (a) Variation in the SBH at the interface between the cathode and TiO_{2-x} with respect to the applied voltage in the second cycle depicted in the inset of Fig. 3(a). (b) Simulated profiles of the conduction-band edge and the Fermi energy at −0.5 V during the second downward sweep (dn2), at −0.5 and (c) 0.5 V during the second upward sweep (up2), and at 0.5 V during the third downward sweep (dn3) in the second cycle. The Fermi energy of the LE is taken as a reference energy. Black and red lines denote high and low resistance states, respectively.

(>1000 °C).[20] The diffusivity of oxygen in Pt was set to 10^{-15} $cm^2\,s^{-1}$.[21]

Calculated J-V hysteresis with two cycles of the applied voltage is plotted in Fig. 4(a). The applied voltage cycle is depicted in the inset of Fig. 4(a). The delay time of each voltage step was 0.1 s. Since the formation and the annihilation of oxygen vacancies at LE/TiO_{2-x} occur with applying a negative and a positive voltage to the RE, respectively, thus set and reset switching occur under negative and positive voltage, respectively, as shown in Fig. 4(a). The set switching in Fig. 4(a) is not very obvious because a gentle decrease in resistance rather than an abrupt step takes place during the set switching. The variation in oxygen-vacancy density at the LE/TiO_{2-x} is shown in Fig. 4(b). The increase in oxygen-vacancy density and thus space charge during the set switching leads to the reduction in the SBH so that current increases with increasing oxygen-vacancy density at that interface. The opposite happens during the reset switching voltage region: Oxygen-vacancy density at the LE/TiO_{2-x} interface decreases giving rise to an increase in the SBH. Therefore, the hysteretic J-V behavior is observed during the reset switching.

In Fig. 4(b), it can be noticed that oxygen-vacancy density as a function of the applied voltage in the second cycle is not completely identical to that in the first cycle, thus the BRS curves in the first and second cycles show a slight difference as shown in Fig. 4(a). The difference of oxygen-vacancy density relying on a cycle number is due to the variation in the Nernst potential V_n of the oxygen-vacancy formation reaction [Eq. (1a)]. As given by Eq. (12), V_n is a function of the density of oxygen vacancies and oxygen ions in the LE. V_n indicates equilibrium voltage. That is, when $V(d_1)$ is equal to V_n, the system reaches equilibrium so that no further changes in the density of the ionic species take place. As $V(d_1)$ is (more) different from V_n in the positive (negative) direction, the oxygen-vacancy annihilation (formation) reaction, the forward (reverse) of Eq. (1a) becomes more accelerated. Therefore, oxygen-vacancy and ion density and V_n influence each other and they show variation in each voltage cycle so that the nonclosed loop of oxygen-vacancy density with respect to the applied voltage shown in Fig. 4(b) was obtained. The variation in oxygen-vacancy and ion densities with respect to a cycle number could be a reason for fatigue of bipolar switching.

The SBH at the interface between the cathode and TiO_{2-x} with respect to the applied voltage is shown in Fig. 5(a). The open symbols on the negative voltage side indicate the SBH at the TiO_{2-x}/RE(cathode) interface and the closed ones on the positive side indicate the SBH at the LE(cathode)/TiO_{2-x} interface. The hysteretic SBH variation shown in Fig. 5(a) plays an essential role in our model of bipolar switching. Compared with the SBH at TiO_{2-x}/RE in the second downward sweep (dn2), a decrease in the SBH in the second upward sweep (up2) can be identified on the negative voltage side of Fig. 5(a). It can be noted that the SBH values under the negative voltage are negative. In spite of the negative SBH electrons depleted in the vicinity of the interface between TiO_{2-x} and the cathode as can be seen near the TiO_{2-x}/LE and RE/TiO_{2-x} interfaces in Figs. 5(b) and 5(c), respectively. That is, the interfaces still play a role in controlling current flow through the cell so that J-V characteristics do not show linear behavior meaning Ohm's law. Comparison between the SBH during dn2 and up2 gives the origin of the set switching. It turns out that after the set switching the SBH becomes more negative so that the number of electrons in the cathode (LE) with energies above the conduction-band minimum of TiO_{2-x} increases. Consequently, the set switching results in a decrease in resistance. Under the positive voltage in up2 another hysteretic SBH at LE/TiO_{2-x} can be observed. Compared with the SBH under the positive voltage during up2, the SBH during the third downward sweep (dn3) is found to increase. The increase in the SBH thus causes an increase in resistance (reset switching).

The conduction-band edge and the Fermi energy profiles at −0.5 V during dn2 and up2 and +0.5 V during up2 and dn3 are plotted in Fig. 5(b). The conduction-band profiles are flat apart from the interface regions regardless of the applied voltage and the resistance state. This is attributed to good electric field screening within a short screening length by a

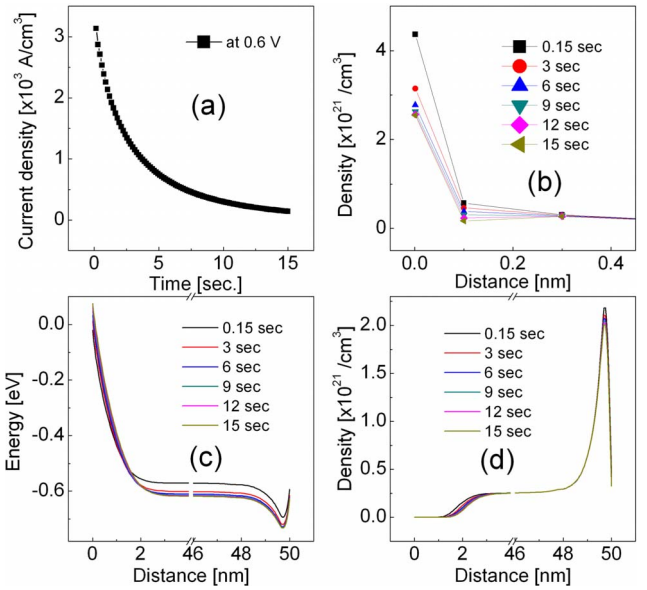

FIG. 6. (Color online) (a) *J-t* curve at an applied voltage of 0.6 V undergoing reset switching. (b) oxygen-vacancy density at the LE/TiO_{2-x} interface, (c) conduction-band minimum profile in TiO_{2-x}, (d) electron distribution profile as a function of a voltage application time at an applied voltage of 0.6 V

large amount of oxygen vacancies in the vicinity of the interfaces so that a voltage is barely applied in the bulk of TiO_{2-x}. Regardless of the applied voltage the Fermi energy is located above the conduction-band edge except for that in the vicinity of the two interfaces, meaning the bulk of TiO_{2-x} has the much higher conductivity so that the bipolar switching is controlled by the interface properties.

The time-dependent variation in current density under a constant voltage of 0.6 V is plotted in Fig. 6(a). The parameters given in Table I were used for the calculation of the current density-time (*J-t*) behavior. This voltage belongs to a reset switching regime so that the current density decreases with respect to time. Corresponding variation in the density of oxygen vacancies in the vicinity of LE/TiO_{2-x} at the same voltage (0.6 V) as a function of time is plotted in Fig. 6(b). The annihilation of oxygen vacancies takes place, thus a number of oxygen vacancies decrease with respect to time. Figures 6(c) and 6(d) depict the conduction-band edge profile and variations in electron density, respectively, with respect to time at 0.6 V.

J-V curves calculated using three different formation energies Δh (0.45, 0.75, and 0.9 eV) for the formation of oxygen vacancies and the corresponding densities of them at LE/TiO_{2-x} are plotted in Figs. 7(a) and 7(b), respectively. The applied voltage cycle is depicted in the inset of Fig. 4(a). The formation energy Δh determines set and reset voltage regimes. By the comparison between the oxygen-vacancy variation curves shown in Fig. 7(b) for 0.75 and 0.9 eV cases, it can be concluded that a lower formation energy shifts voltages for the activation of oxygen-vacancy formation and annihilation reactions to higher values. For the 0.45 eV case the switching voltage regimes are out of the applied voltage range so that no bipolar switching was observed. An increase in oxygen-vacancy density at the LE/TiO_{2-x} interface during the first downward sweep becomes less obvious as the formation energy decreases as shown in Fig. 7(b). A low formation energy means the difference between the energies of the right and the left sides of Eq. (1a) is small. Therefore, to accelerate the reverse reaction of Eq. (1a) for a system with a low formation energy, namely, to increase the energy difference, one should decrease the energy of the right side of Eq. (1a) by applying a negative high voltage to the LE compared with a higher formation case. In fact, for the 0.45 eV case a voltage more negative than −0.8 V was necessary for the activation of oxygen-vacancy formation.

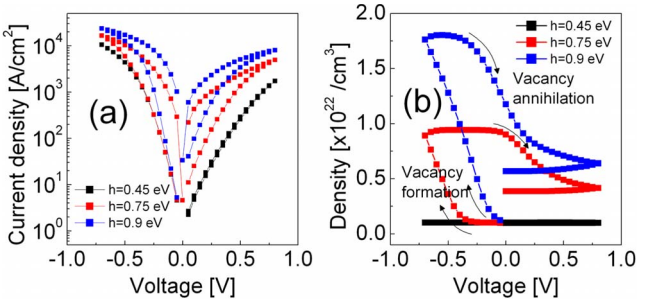

FIG. 7. (Color online) (a) *J-V* curves calculated using a formation energy Δh of 0.45, 0.75, and 0.9 eV. The inset depicts the applied voltage cycle. (b) Corresponding densities of oxygen vacancies at the LE/TiO_{2-x} interface.

For a comparison with experimental results bipolar switching curves measured on a Pt(100 nm)/TiO_2(100 nm)/Pt(100 nm) cell is plotted in Fig. 8. A sample fabrication procedure has been reported elsewhere.[3] The switching curves undergo set and reset switching at negative and positive voltage, respectively. From Figs. 4(a) and 8 the total cross-sectional area of the conduction paths can be roughly determined, where *J-V* and current-voltage (*I-V*) curves are respectively plotted. A calculated cross-sectional area is a few tens of μm^2, as mentioned in Sec. II A. As a matter of fact, this area is well consistent with a value determined experimentally.[6]

The bipolar switching model described up to now leaves many open questions. Concerning the electrochemical reaction of Eq. (1a), for instance, its kinetics has been hardly clarified so that some parameters including k_-^0 at both interfaces, β, and n were speculated. Those parameters should be

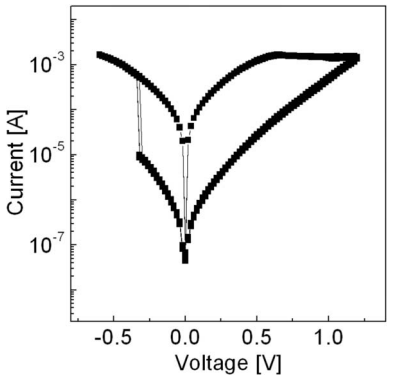

FIG. 8. Bipolar switching curves measured on a Pt(100 nm)/TiO_2(100 nm)/Pt(100 nm) switching cell.

defined for a better description of bipolar switching. In addition, material properties such as ε_{rH} and ϕ_b are not still obvious. More studies on properties of TiO_{2-x} reduced by electroforming should be carried out.

As mentioned in the introduction, the aim of this paper is to propose a prototype of bipolar switching in TiO_2 in terms of oxygen-vacancy-related electrochemical reactions, and thus we simplified our system by dealing with a one-dimensional $Pt/TiO_2/Pt$ junction. This proposed model itself is barely able to explain many technical issues such as long data retention, endurance, switching speed and so on. These issues should be approached with taking into account the three-dimensional distribution of conduction paths because their properties are determined by three-dimensionally located conduction paths. However, in this paper we only describe bipolar switching with one conduction path. Therefore, the model needs to be elaborated in order to describe the reality of RRAM devices.

III. CONCLUSIONS

A bipolar switching mechanism in a $Pt/TiO_2/Pt$ switching cell after asymmetric electroforming is suggested in terms of oxygen-related electrochemical reactions, oxygen-vacancy formation, and annihilation reactions at one of the Pt/TiO_2 interfaces, which is activated by the polarity of the asymmetric electroforming process. By taking into account the Helmholtz layer at the active interface the reaction constants for the formation and the annihilation of oxygen vacancies are expressed as a function of the applied voltage, thus the density of oxygen vacancies is given with respect to the applied voltage. The variation in oxygen-vacancy density at the active interface leads to a change in the SBH, consequently, giving rise to a transient resistive switching relying on the polarity of the applied voltage.

ACKNOWLEDGMENTS

One of the authors (D.S.J.) would like to thank the Deutscher Akademischer Austausch Dienst (DAAD) for the scholarship supporting his research at the Forschungszentrum Jülich GmbH. The authors thank P. Meuffels for fruitful discussions.

*Permanent address: Thin Film Materials Research Center, Korea Institute of Science and Technology, Seoul 136-791, Republic of Korea; dsjeong@kist.re.kr

[1] D. S. Jeong, H. Schroeder, and R. Waser, Electrochem. Solid-State Lett. **10**, G51 (2007).
[2] J. J. Yang, M. D. Pickett, X. Li, D. A. A. Ohlberg, D. R. Stewart, and R. S. Williams, Nat. Nanotechnol. **3**, 429 (2008).
[3] H. Shima, N. Zhong, and H. Akinaga, Appl. Phys. Lett. **94**, 082905 (2009).
[4] K. Szot, W. Speier, G. Bihlmayer, and R. Waser, Nature Mater. **5**, 312 (2006).
[5] M. Janousch, G. I. Meijer, U. Staub, B. Delley, S. F. Karg, and B. P. Andreasson, Adv. Mater. **19**, 2232 (2007).
[6] D. S. Jeong, H. Schroeder, U. Breuer, and R. Waser, J. Appl. Phys. **104**, 123716 (2008).
[7] R. Waser and M. Aono, Nature Mater. **6**, 833 (2007).
[8] M. Radecka and M. Rekas, J. Eur. Ceram. Soc. **22**, 2001 (2002).
[9] V. E. Henrich and P. A. Cox, *The Surface Science of Metal Oxides*, 1st ed. (Cambridge University Press, Cambridge, 1994).
[10] E. Cho, S. Han, H.-S. Ahn, K.-R. Lee, S. K. Kim, and C. S. Hwang, Phys. Rev. B **73**, 193202 (2006).
[11] C. H. Hamann, A. Hamnett, and W. Vielstich, *Electrochemistry*, 2nd ed. (Wiley-VCH, Weinheim, 2007).
[12] S. H. Jeon, B. H. Park, J. Lee, B. Lee, and S. Han, Appl. Phys. Lett. **89**, 042904 (2006).
[13] W. X. Li, L. Österlund, E. K. Vestergaard, R. T. Vang, J. Matthiesen, T. M. Pedersen, E. Lægsgaard, B. Hammer, and F. Besenbacher, Phys. Rev. Lett. **93**, 146104 (2004).
[14] U. Balachandran and N. G. Eror, J. Mater. Sci. **23**, 2676 (1988).
[15] C. R. Crowell and M. Beguwala, Solid-State Electron. **14**, 1149 (1971).
[16] K. W. Morton and D. F. Mayers, *Numerical Solution of Partial Differential Equations, An Introduction* (Cambridge University Press, Cambridge, 2005).
[17] W. H. Press, S. A. Teukolsky, W. T. Vetterling, and B. O. Flannery, *Numerical Recipes in C: The Art of Scientific Computing*, 2nd ed. (Cambridge University Press, Cambridge, 1992).
[18] S. M. Sze, *Physics of Semiconductor Devices* (Wiley, New York, 2007).
[19] C. T. Black and J. J. Black, IEEE Trans. Electron Devices **46**, 776 (1999).
[20] D.-K. Lee and H.-I. Yoo, Solid State Ionics **177**, 1 (2006).
[21] L. R. Velho and R. W. Bartlett, Metall. Trans. **3**, 65 (1972).
[22] Measured dielectric constant of TiO_2. Not published value.
[23] S. O. Kasap, *Principle of Electronic Materials and Devices*, 2nd ed. (McGraw-Hill, New York, 2002).
[24] J. A. Becker, Rev. Mod. Phys. **7**, 95 (1935).